

Controls on the runoff response of the ephemeral Arroyo de los Pinos watershed to high-intensity rain

Daniel Cadol, New Mexico Tech, Socorro, NM, daniel.cadol@nmt.edu

Sandra Glasgo, WSP, Inc., Redmond, WA, sandry1616@gmail.com

Madeline Richards, ERM, Inc., Walnut Creek, CA, maddiear@gmail.com

Kyle Stark, San Francisco Estuary Institute, Richmond, CA, kstark131@gmail.com

Loc Luong, New Mexico Tech, Socorro, NM, loc.luong@student.nmt.edu

Susan Bilek, New Mexico Tech, Socorro, NM, susan.bilek@nmt.edu

David Varyu, United States Bureau of Reclamation, Denver, CO, dvaryu@usbr.gov

Jonathan B. Laronne, Ben Gurion University of the Negev, Beer Sheva, Israel, john@bgu.ac.il

Abstract

The relative influence of rainfall and watershed characteristics in controlling runoff in ephemeral channel systems is difficult to interrogate with current field datasets. First, runoff-producing rainstorms are rare in the environments that host ephemeral channels. Compounding this, there are at least three dimensions of variability in rainfall that affect runoff: rainfall intensity, total depth of high-intensity rainfall (or, equivalently, duration of high-intensity rainfall), and spatial extent of high-intensity rainfall. As a result, there is rarely enough field data to fully cover this variable space. Beyond this, lithology, vegetation, and soil all affect infiltration – both on hillslopes and in channels – and these influences are difficult to quantify using sparse field measurements.

We are developing a new runoff and rainfall monitoring dataset for the Arroyo de los Pinos watershed in central New Mexico to help bridge this gap. Our goal is to use the diverse geology of the basin to advance understanding of runoff generation and channel conveyance loss. The 32 km² watershed has three important lithologic groupings: limestone bedrock, sandstone-shale bedrock, and weakly-lithified alluvial basin fill. Here, we present two years of monitoring data from this watershed. Runoff only occurs during the summer monsoon season, in instances when high-intensity thunderstorms linger over the watershed for sufficiently long durations. An approximate 15-minute rain intensity threshold for runoff production was observed to be 0.2 mm/min. Runoff is produced most readily in limestone sub-basins, followed by sandstone, and least by alluvial fill, a pattern that is consistent with the increasing hydraulic conductivity of the three lithologies in that order. Rainfall intensity is a stronger predictor of the runoff ratio than rainfall depth, particularly in smaller subbasins and in limestone-dominated subbasins. This is consistent with observations of infiltration-excess overland flow throughout the watershed during high-intensity storms. In general, larger subbasins have lower runoff ratios, due to high transmission losses (i.e., bed infiltration) in the ephemeral channel network. However, the mix of lithologies in the larger subbasins complicates the interpretation.

Introduction

Runoff from basins drained by ephemeral channels is generated in a particularly non-linear manner. Typically, rainfall intensity in excess of infiltration capacity is the dominant control, as infiltration-excess overland flow (Horton, 1945) contributes rapid hillslope runoff that can trigger damaging flash floods. Additional controls include watershed area and channel transmission losses (Greenbaum, et al., 1998; Dunkerley & Brown, 1999; Dahan et al., 2007; Goodrich et al., 2013).

The relative influence of rainfall characteristics versus watershed characteristics in controlling runoff production in ephemeral channel systems is difficult to interrogate with field data. First, runoff-producing rainstorms are rare in the environments that host ephemeral channels. Compounding this, there are at least three dimensions of variability in rainfall that affect runoff: rainfall intensity (Sharon, 1972; Marra and Morin, 2018), total depth of high-intensity rainfall (or, equivalently, duration of high-intensity rainfall; Kampf et al, 2018), and spatial extent of high-intensity rainfall (Belachsen et al., 2017). As a result, there are rarely enough data to fully cover this variable space. Long-term monitoring is required, but long-term research stations are site-specific by their nature. The influence of watershed size can be investigated in most long-term research stations by monitoring nested subbasins. But the influences of lithology, vegetation, and soil on infiltration – both on hillslopes and in channels – are difficult to include. The establishment of dryland research watersheds in unstudied and diverse lithologies, in combination with those already established, such as the Nahal Yael (Bahat et al., 2009) and Walnut Gulch (e.g., Goodrich et al., 2013), can help bridge this gap.

Our objective in this study was to explore the relative influence of subbasin drainage area, rainfall depth, rainfall intensity, and subbasin lithology in controlling the runoff ratio and runoff depth in the Arroyo de los Pinos watershed in central New Mexico. We hypothesized (i) that rainfall intensity would be more influential in producing runoff than total rainfall depth, based on the predominance of infiltration-excess overland flow; (ii) that lithology would be an important secondary control, with limestone-dominated watersheds producing more runoff than those dominated by sandstone and shale or those with extensive alluvial cover, based on their relative hydraulic conductivities; and (iii) that controls on runoff production that scale with watershed area (e.g., channel infiltration) would interact with basin lithology, leading to lower runoff ratios in larger watersheds of a given lithology.

Study site

The Arroyo de los Pinos is a 32 km² watershed located near Socorro, New Mexico, USA, and is a tributary to the Rio Grande (Figure 1). The climate is semiarid, with ~ 250 mm of average annual rainfall. The majority of this rain typically falls during the summer monsoon season. The Pinos watershed is at the northern edge of the Chihuahuan Desert, and is host to desert shrubs and cacti such as creosote, mesquite, tarbrush, cholla, prickly pear, and ocotillo. Cottonwood and juniper trees are sparsely scattered along tributaries and main channel banks.

The varied lithology underlying the Pinos sets it apart from the few other semiarid or arid watersheds that currently have extensive rainfall and runoff monitoring networks. At the outlet

where the Pinos joins the Rio Grande, Holocene alluvium, mud, and sand are predominant. Aeolian sand-sheets blanket the lower-elevation drainage divides. The bottom third of the watershed overlies the Pliocene to middle-Pleistocene Sierra Ladrones Formation, which is part of the Santa Fe Group, characterized by poorly sorted conglomerate and medium to coarse cross-bedded sandstone. Upper-Pleistocene young valley alluvium overlays the conglomerate/sandstone facies along the braided lower reach of the Arroyo de los Pinos.

The middle portions of the watershed are dominated by the Pennsylvanian Madera Group, made up of the Atrasado and Gray Mesa Formations. These units are predominantly a cliff-forming fossiliferous marine limestone in this area, but include interbedded mudstone and sandstone.

The north-central portion of the basin has a region dominated by the Permian Yeso and Abo Formations, and the Permian-Pennsylvanian Bursum Formation. The Yeso formation consists of interbedded sandstone, siltstone, mudstone, and dolomitic limestone. The Abo Formation is an interbedded shale, mudstone, and siltstone, with thin conglomerate beds. The Bursum Formation is interlayered with the Abo and Atrasado, and primarily consists of mudstone with some thin limestone layers. The eastern, upstream-most portion of the basin exposes a mix of the Atrasado, Abo, and Bursum Formations, with low-gradient areas overlain by quaternary alluvium.

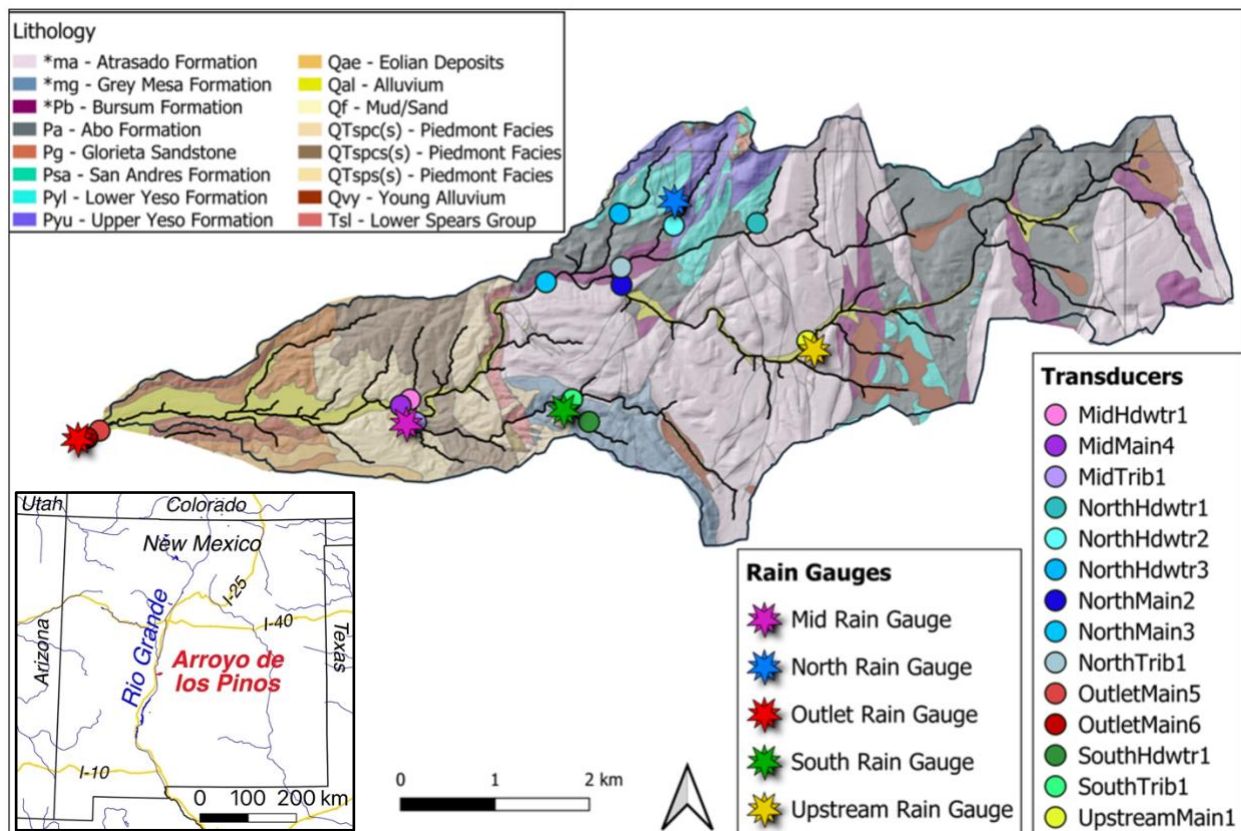


Figure 1. Study site location within New Mexico (inset) and lithology of the Arroyo de los Pinos watershed. Rain gauge and pressure transducer locations are marked as stars and circles, respectively. Geologic mapping by Cather and Colpitts (2005, 2012) and Cather et al. (2004, 2014).

Methods

Rainfall and runoff monitoring equipment was installed in the Pinos watershed in 2019 (Richards, 2020). Rainfall was measured with five tipping-bucket rain gauges located in accessible areas of the watershed that allowed for adequate coverage of each subbasin. The naming convention for the rain gauges indicates the area of the watershed where the gauge is located: Outlet, Mid, South, North, and Upstream (Figure 1). The Upstream gauge recorded at a 1-minute interval, the Outlet at a 15-minute interval, and the other three at 5-minute intervals. Data were manually downloaded every one-to-two months during monsoon season and once during the winter season. Storm total rainfall and peak 10- to 15-minute rainfall intensity for all runoff producing events were extracted from the time series at each gauge. The rain gauge network spacing of 6.4 km²/gauge is intermediate to the 0.6 km²/gauge spacing in Walnut Gulch Experimental Watershed in Arizona (Goodrich et al., 2021) and the 26 km²/gauge spacing in Nahal Yael in Israel (Bahat et al., 2009). Both of these watersheds differ from the Arroyo de los Pinos due to their moderately homogeneous lithology.

An average rainfall depth was calculated using the Thiessen polygon method for each subbasin, i.e., mapping the area of influence for each of the five rain gauges as the area over which that gauge was the nearest. A weighted average of the rainfall recorded at each gauge that had an influence area covering part of the subbasin was calculated, with weighting factors assigned based on the fraction of the subbasin area within the area of influence for that gauge. Maximum rainfall intensity for each subbasin was assigned as the maximum 10- to 15-minute intensity recorded at any of the gauges that had areas of influence covering part of that subbasin.

Flow stage was monitored at 13 cross sections within the channel network using unvented pressure transducers (Hobo U20). Due to equipment damage, battery failure, and the installation of new sites over time, the number of transducers operating during any given flood varied (10-13). The naming convention follows the same spatial pattern as that of the rain gauges, wherein the first preface identifies the area of the watershed (Upstream, North, South, Mid, and Outlet), the next set of letters identifies the type of channel in which the transducer was placed (Main – main channel, Trib – tributary of moderate size, Hdwtr – small head water channel), and the last number identifies the position within the subbasin, or in the full basin for Main channels – 1 in the east, increasing to the west (Figure 1). Where possible, transducers were deployed in 2.5-cm-diameter holes drilled into bedrock or immobile boulders, and elsewhere they were deployed in perforated steel pipes driven into the alluvium. Three transducers were placed outside the channels to monitor the barometric pressure at various elevations in the watershed, which allowed for barometric compensation of the pressures recorded within the channel during flow events. Each logger recorded at 3-minute intervals during the 2020 monsoon season (Richards, 2020), 2-minute intervals during the 2021 monsoon season (Glasgo, 2022), and 5-minute intervals during the off-season. The pressure data (kPa) were corrected using the barometric data, and converted to depth (m) using standard values for water density (1000 kg/m³) and gravity.

Flow depth data were converted to discharge estimates using the Manning equation:

$$Q = A \frac{1}{n} R_h^{2/3} S_f^{1/2} \quad (1)$$

where Q is the volumetric discharge, A is the cross-sectional area of flow, n is the Manning roughness coefficient, R_h is the hydraulic radius, and S_f is the energy slope. Cross-sectional area and hydraulic radius were calculated using surveyed channel cross sections at each pressure

transducer and the measured depth of flow (d) from the transducers. Energy slope was approximated using the average surveyed channel bed slope over ~ 100 m of channel length, centered on the transducer. The Manning roughness coefficient was estimated using an empirical equation (Leopold and Wolman, 1957) relating the Darcy-Weisbach friction factor (f) to the hydraulic radius and roughness coefficient:

$$n = 0.2626R_h^{1/6} \sqrt{\frac{f}{8}} \quad (2)$$

The Darcy-Weisbach friction factor can be empirically related to the 84th percentile grain size diameter (D_{84}) using the equation (Ferguson, 2007):

$$\frac{f}{8} = \frac{\left(\frac{D_{84}}{R_h}\right)^b}{a^2} \quad (3)$$

where the exponent b is $1/3$ for deep flows and 2 for shallow flows. The empirical constant a also varies with flow depth, and is approximated as 7.5 for deep flows and 2.5 for shallow flows (Ferguson, 2007). The division between shallow and deep flows is determined by the relative submergence of the D_{84} grain, with the deep flow equation used if $d/(D_{84}) > 4$ (Ferguson, 2007). The D_{84} grain diameter was determined by conducting a Wolman pebble count at each cross section, wherein 100 randomly selected clasts were measured (Wolman, 1954).

Runoff ratio was calculated as the runoff volume divided by the rainfall volume, for each subbasin during each storm event. Rain depth and runoff depth are equal to the relevant rain volume and runoff volume divided by subbasin area.

Results

We obtained data on eleven flow-producing rainfall events – three in 2020 and eight in 2021 (Glasgo, 2022). Only monsoon season storms produced flow. There were a variety of storm movement patterns, with storms approaching the watershed from every cardinal direction. We do not attempt to ascertain the influence of storm-track direction in this analysis. Likewise, storm velocity varied greatly, and was reflected in the duration of each storm, and thereby in the total depth of rainfall. The spatial distribution of rain also varied, and this was accounted for in the differing rainfall depths reported for each subbasin in any given storm. Some storms only crossed part of the watershed, such as the southward-traveling event of 2 July, 2021, in which little to no rainfall was recorded at the Upstream and North rain gauge, yet 23 mm were recorded at the Outlet rain gauge. Due to the weighting-by-area of the rain gauges in calculating rainfall depth for each subbasin, the larger subbasins in storms such as these were assigned depths that averaged across areas of varying rainfall. Single-event rainfall, averaged across the five gauges, ranged from 37 mm (5 July, 2021) to 5 mm (28 Sept, 2021) for the eleven runoff producing events (Table 1).

Runoff depth increased with rainfall depth, as expected (Figure 2), and although the correlation is highly significant ($p < 0.001$), the predictive power is low ($R^2 = 0.27$). There is a weak pattern of smaller watersheds having slightly higher runoff depth for a given rainfall depth, which is of marginal statistical significance when included in a multiple linear regression ($p = 0.07$), but it adds very little predictive power beyond the single linear regression (multiple- $R^2 = 0.29$).

Table 1. Rainfall at each of the five rain gauges during the eleven runoff producing storm events

Date (Y.M.D)	Outlet (mm)	Mid (mm)	South (mm)	North (mm)	Upstream (mm)
2020.07.23	10	16	13	28	*
2020.07.24	16	30	23	17	*
2020.09.01	13	11	7	4	3
2021.07.02	23	6	1	0	0
2021.07.05	32	38	28	57	27
2021.07.06	36	25	31	28	24
2021.07.23	37	20	24	11	29
2021.08.12	18	13	15	5	7
2021.08.23	21	15	15	6	12
2021.08.27	21	21	16	6	13
2021.09.28	2	*	5	6	10

* Gauge was not operational during this event.

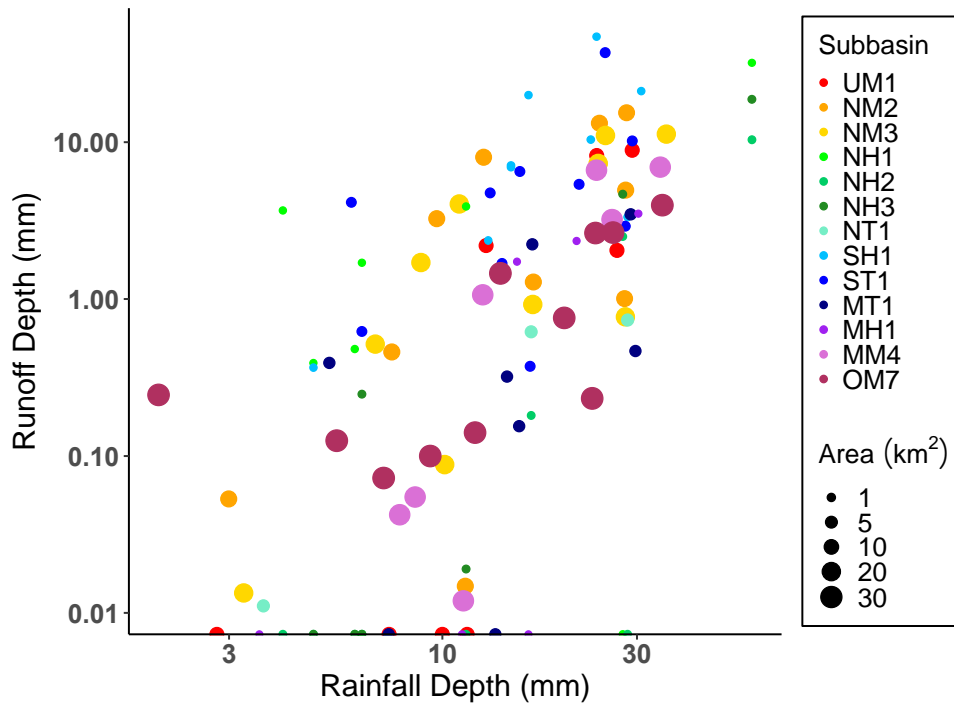


Figure 2. Runoff depth vs. rainfall depth for each storm event at each Pinos subbasin. Subbasin-event combinations that produced zero runoff are plotted along the x-axis. Point size reflects subbasin area.

The influence of lithology is most readily apparent when focusing on small subbasins. We calculated the average runoff ratio (percent of precipitation that becomes runoff) for each of the thirteen subbasins with valid runoff data from at least seven of the eleven flow events. This average includes events with documented zero runoff, but excludes periods when the transducer was not operational. The two highest runoff ratios derived from the two subbasins with full limestone exposure (Figure 3). The next highest runoff ratios belong to the subbasins with a mix of limestone and clastic (i.e., sandstone & shale) lithology. Purely clastic subbasins and

subbasins with high alluvium influence had the lowest average runoff ratios. Overlaid on this relationship between runoff and lithology was a pattern of lower runoff ratios in larger watersheds (Figure 3), although as lithologies become more mixed at the largest drainage areas, subbasin categorization becomes more arbitrary, and the pattern becomes weaker.

Including rainfall intensity as a predictor of runoff ratio or runoff depth considerably increased predictive power (Figure 4). The positive correlation (Pearson coefficient) within any lithologic class between runoff ratio and rainfall intensity was strong, ranging from $r=0.76$ for limestone to $r=0.35$ for limestone/clastic mix. The slopes of the trends (i.e., the regression parameter estimates) range from a runoff ratio increase of 35% per mm/min of rain intensity for alluvium to a runoff ratio increase of 80% per mm/min of rain intensity for limestone (Figure 4). Three events in the limestone-dominated watersheds produced runoff ratios over 100%. Such values are not physically possible, and reflect uncertainty in the runoff estimation using the Manning equations (Eq. 1) and potential error in rainfall depth averaging using the Thiessen polygon method. However, the data were retained because they provide real insight into the relationship trend between rainfall intensity and runoff ratio despite the high uncertainty.

The multiple linear regression analysis identified rainfall intensity as the most influential rain parameter for predicting various runoff metrics. The regression to predict runoff ratio using rain depth, area, and lithology produced a multiple- R^2 of 0.31, while the regression to predict runoff ratio using rain intensity, area, and lithology produced a multiple- R^2 of 0.42. When both rain depth and intensity were included in the regression, along with area and lithology, intensity was highly significant ($p < 0.001$), while rain depth was not ($p = 0.50$). Lithology was a very important co-predictor. A regression predicting runoff ratio with intensity alone produced an $R^2 = 0.14$, while adding lithology to the regression increased it to $R^2 = 0.41$. Subbasin area added little predictive power to this regression (as seen by the small difference relative to the R^2 of 0.42 reported above), but it was marginally significant statistically ($p=0.12$) and had a negative regression parameter, indicating lower runoff ratios in larger watersheds, as is expected in the presence of flow transmission loss and related processes.

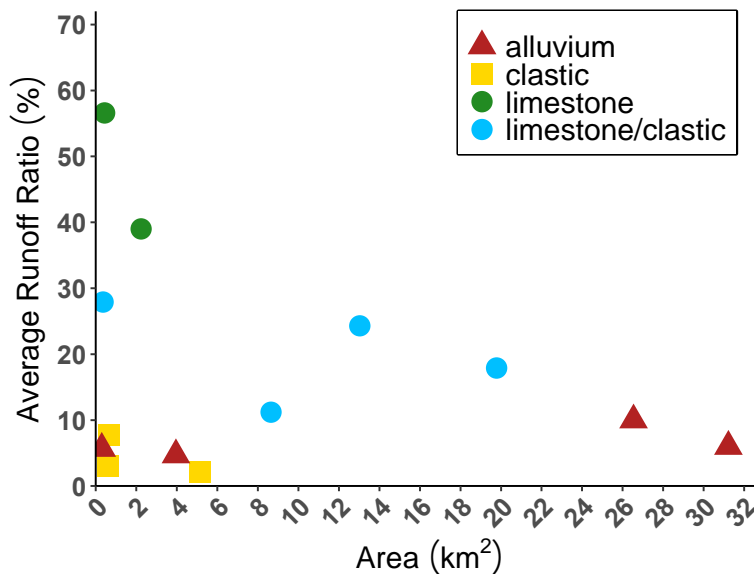


Figure 3. The variation of average runoff ratio at each transducer site with subbasin area, grouped by subbasin lithology. Clastic lithology refers to sandstone, siltstone, and mudstone. Alluvial lithology applies to stations near the outlet that are locally dominated by alluvium but that also drain the whole basin.

Multiple regressions to predict runoff depth had similar predictive strength. The full regression, predicting runoff depth using rainfall intensity, rainfall depth, area, and lithology had a multiple- R^2 of 0.50, with significant or marginally-significant p-values for all four predictors and parameter estimates that are consistent with process-based expectations (Table 2). Removing rainfall depth increased all remaining p-values, and decreased the multiple- R^2 to 0.46. Together, these regressions indicate that, within our dataset, rainfall intensity is a more powerful predictor of runoff than rainfall depth (though they do not necessarily contain redundant information), and that lithology is more influential than basin area.

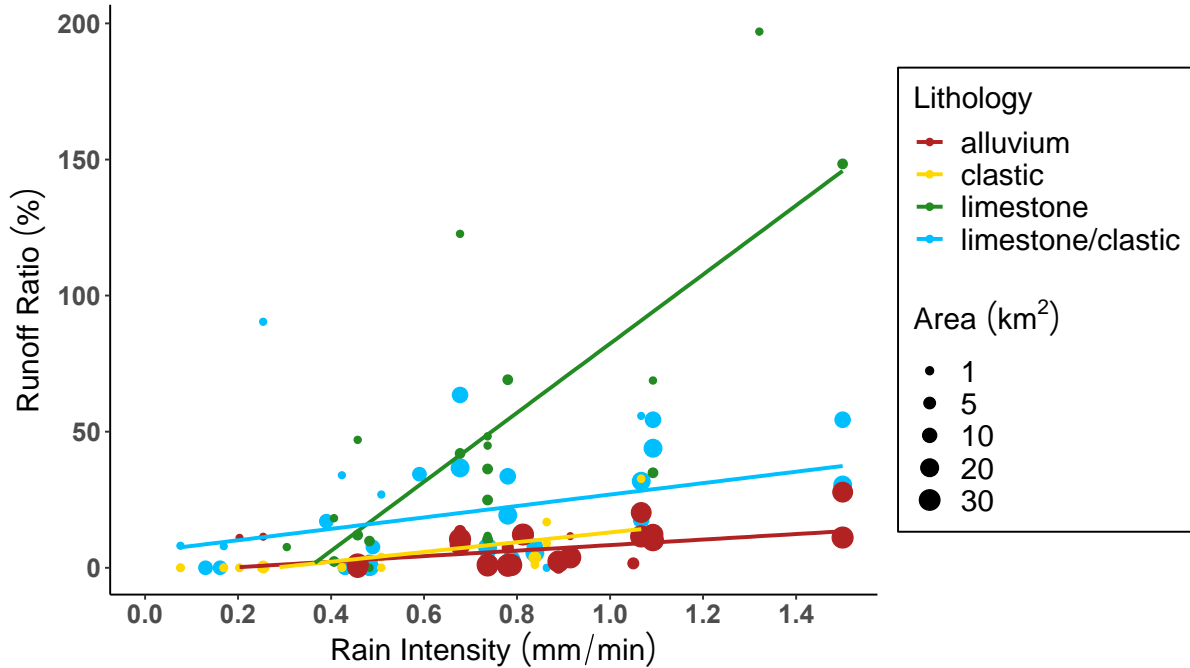


Figure 4. Runoff ratio of individual flow events in each subbasin as a function of maximum 10- to 15-minute rainfall intensity measured at rain gauges near the subbasin. Points are colored by dominant subbasin lithology and sized by subbasin area. Trend lines are least-squares regression fits, with 90% confidence interval shown in gray. Runoff ratios above 100% are presumed to be due to runoff volume estimation uncertainty and limited spatial representativeness of point rain gauge data for the subbasin.

Table 2. Parameter estimates and p-values for regression of Runoff Depth using Rain Intensity, Rain Depth, Area, and Lithology as predictors.

Predictor	Parameter Estimate	P-value
(intercept)	-6.95	0.0002
Rain Intensity	9.07	0.0001
Rain Depth	0.16	0.01
Area	-0.10	0.12
Lith ¹ (clastic)	1.39	0.47
Lith (limestone/clastic)	3.28	0.02
Lith (limestone)	7.22	0.0002

¹Alluvium is the baseline model lithologic class (parameter estimate = 0).

Discussion and Conclusions

The predominance of rainfall intensity over rainfall depth in predicting runoff is consistent with the previously reported and locally observed dominance of infiltration-excess overland flow in semi-arid regions. We observed overland flow on hillslopes of diverse gradients throughout the watershed, even in the downstream areas where the underlying lithology is poorly consolidated alluvial fan deposits of the Santa Fe Group. The rainfall intensities were all high during observed overland flow on hillslopes, and the spatial distribution of runoff was inconsistent with saturation-from-below processes that might indicate saturation-excess overland flow.

Even when rain intensity is accounted for in the prediction of runoff depth, rain depth is still a statistically significant predictor (Table 2). The parameter estimate for rain depth is positive, indicating that more rain produces more runoff, even after accounting for rain intensity. This may be related to the limitations of using a 10- to 15-minute maximum intensity value. If that intensity is maintained longer, we should expect more runoff for the same maximum intensity. There were some cases where the peak intensity was maintained longer than 15 minutes, but it was rare in our dataset. The statistical results, while being consistent with theoretical considerations, may also be spurious due to multi-collinearity. Rainfall intensity was correlated with rainfall depth (Pearson $r = 0.63$, $R^2 = 0.39$), so including both as simultaneous predictors has the potential to produce spurious results. Given the logic of the outcome, however, it seems reasonable to infer that there is some additional relevant information contained in the rain depth data that is not redundant with rain intensity.

The high runoff production in the limestone areas of the Arroyo de los Pinos is most likely associated with limited soil development on the hillslopes and thinner alluvial accumulations in the channels. The dry climate limits limestone dissolution rates and slows karstification. The runoff influence of particular lithologies likely differs in other climates, for example, in areas where limestone watersheds experience flow loss to the subsurface through karst conduits.

Nonetheless, within our watershed, the lithologic influence is clear. Clastic (i.e., sandstone and siltstone) dominated areas produce much less runoff than limestone-dominated areas, and subbasins that have a mix of these two lithologies are intermediate, though weighted somewhat toward the clastic trends (Table 2). All three produce more runoff than poorly-consolidated alluvial fan material, results that are consistent with the inferred hydraulic conductivity of the materials.

Additional monitoring in the coming years will enable the collection of a larger dataset over a wider range of rainfall conditions that we hope will enable more robust statistical analysis. Additional instrumentation, for instance, placing rainfall recorders in the uppermost watersheds, will facilitate understanding spatial trends. Further analyses of rainfall intensity may require recording rainfall at higher resolution, as shorter bursts may be important to runoff generation yet remain unobserved in our 10-minute resolution data. Additionally, storm track direction could begin to be separated when sufficient examples are made available of each directionality to allow adequate sample size for statistical analysis. Nonetheless, this initial analysis provides support for two of our hypotheses: 1) that rainfall intensity is more influential in runoff production than rainfall depth, and 2) that limestone-dominated subbasins produce more runoff, whereas unconsolidated alluvium produces less. The influence of basin size is difficult to evaluate due to the mixed lithology of the larger subbasins, but is consistent with larger areas producing lower runoff ratios.

References

- Bahat, Y., T. Grodek, J. Lekach, and E. Morin. 2009. Rainfall–runoff modeling in a small hyper-arid catchment. *Journal of Hydrology*, 373(1-2):204–217. doi: 10.1016/j.jhydrol.2009.04.026.
- Belachsen, I., Marra, F., Peleg, N., & Morin, E. 2017. Convective rainfall in a dry climate: Relations with synoptic systems and flash-flood generation in the Dead Sea region. *Hydrology and Earth System Sciences*, 21(10), 5165–5180. doi: 10.5194/hess-21-5165-2017
- Dahan, Y. Shani, Y. Enzel, Y. Yechieli, and A. Yakirevich. 2007. Direct measurements of floodwater infiltration into shallow alluvial aquifers. *Journal of Hydrology*, 344(3-4):157–170. doi: 10.1016/j.jhydrol.2007.06.033.
- Dunkerley, D., & Brown, K. 1999. Flow behaviour, suspended sediment transport and transmission losses in a small (sub-bank-full) flow event in an Australian desert stream. *Hydrological Processes*, 13, 1577 – 1588.
- Ferguson, R. 2007. Flow resistance equations for gravel- and boulder-bed streams. *Water Resources Research*, 43(5). doi: 10.1029/2006WR005422.
- Glasgo, S. 2022. Connectivity and rainfall-runoff relationships in flashy ephemeral systems. Thesis. New Mexico Institute of Mining and Technology.
- Goodrich, D. C., P. Heilman, M. Nearing, M. Nichols, R. L. Scott, C. J. Williams, and J. Biederman. 2021. The USDA-Agricultural Research Service’s long term agro-ecosystems Walnut Gulch Experimental Watershed, Arizona, USA. *Hydrological Processes*, 35(9), doi: 10.1002/hyp.14349.
- Goodrich, D. C., Williams, D. G., Unkrich, C. L., Hogan, J. F., Scott, R. L., Hultine, K.R., Pool, D., Goes, A. L., & Miller, S. 2013. Comparison of methods to estimate ephemeral channel recharge, Walnut Gulch, San Pedro River Basin, Arizona. *Groundwater Recharge in a Desert Environment: The Southwestern United States*, 9, 77–99.
- Greenbaum, N., Margalit, A., Schick, A., Sharon, & D., Baker, V. 1998. A high magnitude storm and flood in a hyperarid catchment, Nahal Zin, Negev Desert, Israel. *Hydrological Processes*, 12, 1–23.
- Horton, R.E. 1945. Erosional development of streams and their drainage basins: hydrophysical approach to quantitative morphology. *Bulletin of the Geological Society of America* 56, 275-370.
- Kampf, S. K., Faulconer, J., Shaw, J. R., Lefsky, M., Wagenbrenner, J. W., & Cooper, D. J. 2018. Rainfall thresholds for flow generation in desert ephemeral streams. *Water Resources Research*, 54, 9935–9950. doi: 10.1029/2018WR023714
- Marra, F., & Morin, E. 2018. Autocorrelation structure of convective rainfall in semiarid-arid climate derived from high-resolution X-Band radar estimates. *Atmospheric Research*, 200, 126–138. doi: 10.1016/j.atmosres.2017.09.020
- Richards, M.A. 2022, Rainfall-Runoff Relationships in the Arroyo De Los Pinos Socorro New Mexico. Thesis. New Mexico Institute of Mining and Technology.
- Sharon, D., 1972. The spottiness of rainfall in the desert area. *Journal of Hydrology*, 17, 161–175.
- Wolman, G. A. 1954. Method of Sampling Coarse River-Bed Material. *Transactions, American Geophysical Union*, 35(6):951–956.